THE JOURNAL OF PHYSICAL CHEMISTRY C
A JOURNAL OF THE AMERICAN CHEMICAL SOCIETY

pubs.acs.org/JPCC
Article

Reactive Force Field Development for Propane Dehydrogenation on Platinum Surfaces

Published as part of The Journal of Physical Chemistry C virtual special issue "Recent Advances in Simulation Software and Force Fields".

Antoni Salom-Català,[§] Evgenii Strugovshchikov,[§] Kamila Kaźmierczak, Daniel Curulla-Ferré,* Josep M. Ricart,* and Jorge J. Carbó*

Cite This: *J. Phys. Chem. C* 2024, 128, 2844−2855

Read Online

ACCESS | Metrics & More | Article Recommendations | Supporting Information

ABSTRACT: Propane dehydrogenation (PDH) is an on-purpose catalytic technology to produce propylene from propane that operates at high temperatures, 773−973 K. Several key industry players have been active in developing new catalysts and processes with improved carbon footprint and economics, where Pt-based catalysts have played a central role. The optimization of these catalytic systems through computational and atomistic simulations requires large-scale models that account for their reactivity and dynamic properties. To address this challenge, we developed a new reactive ReaxFF force field (**2023-Pt/C/H**) that enables large-scale simulations of PDH reactions catalyzed on Pt surfaces. The optimization of force-field parameters relies on a large training set of density functional theory (DFT) calculations of Pt-catalyzed PDH mechanism, including geometries, adsorption and relative energies of reaction intermediates, and key C−H and C−C bond-breaking/forming reaction steps on the Pt(111) surface. The internal validation supports the accuracy of the developed **2023-Pt/C/H** force-field parameters, resulting in mean absolute errors (MAE) against DFT data of 14 and 12 kJ mol^{-1} for relative energies of intermediates and energy barriers, respectively. We demonstrated the applicability of the **2023-Pt/C/H** force field with reactive molecular dynamics simulations of propane on different Pt surface topologies and temperatures. The simulations successfully model the formation of propene in the gas phase as well as competitive, unproductive reactions such as deep dehydrogenation and C−C bond cleavage that produce H, C_1 and C_2 adsorbed species responsible of catalytic deactivation of Pt surface. Results show the following reactivity order: Pt(111) < Pt(100) < Pt(211), and that for the stepped Pt(211) surface, propane activation occurs on low-coordinated Pt atoms at the steps. The measured selectivity as a function of surface topology follows the same trend as activity, the Pt(211) facet being the most selective. The **2023-Pt/C/H** reactive force field can also describe the increase of reactivity with the temperature. From these simulations, we were able to estimate the Arrhenius activation energy, 73 kJ mol^{-1}, whose value is close to those reported experimentally for PDH catalyzed by large, supported Pt nanoparticles . The newly developed **2023-Pt/C/H** reactive force field can be used in subsequent investigations of different Pt topologies and of collective effects such as temperature, propane pressure, or H surface coverage.

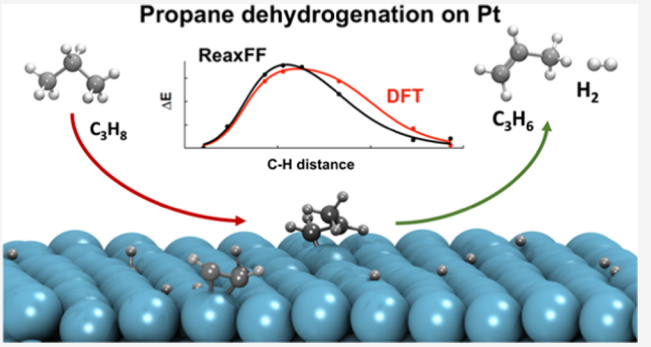

INTRODUCTION

Over the past few years, the demand for light olefins has increased because of their extensive use as chemical building blocks employed in the production of a vast array of essential chemicals such as polymers, oxygenates, and other important chemical intermediates such as ethylbenzene and propionaldehyde.[1−3] Among different possible olefins, propene has become one of the most valuable chemical precursors, with a continuously growing demand, used to synthesize polypropylene, acrylonitrile, and propylene oxide.[4]

Typically, light olefins are obtained by steam cracking or fluid catalytic cracking methods of naphtha, light diesel, and other oil byproducts.[5,6] However, there are limitations to using these methods, such as high-energy demand resulting in a large carbon footprint, low selectivity toward the desired olefin, dwindling petroleum reserves, or rising oil prices. Thus, the use of more efficient conversion methods and technologies is

Received: October 29, 2023
Revised: January 11, 2024
Accepted: January 18, 2024
Published: February 9, 2024

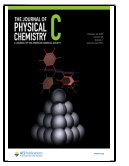

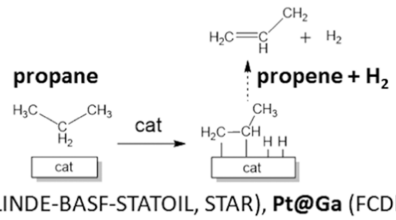

Figure 1. Schematic illustration of the catalytic direct PDH with commercial catalysts used nowadays in the industry.[4]

mandatory. Within this context, the catalytic propane dehydrogenation (PDH) is a convenient process for selective propylene production.[7,8] As shown in Figure 1, this reaction allows obtaining propene and hydrogen directly from propane with no other reagents.[9] Due to the stable and nonpolar nature of alkanes,[10−12] the PDH reaction is endothermic (ΔH^0 = +124 kJ mol^{-1} at 298 K), and therefore, it requires high temperatures (773−973 K) and the presence of a catalyst to be commercially feasible. The widely used catalysts for these processes are metal oxides, typically based on chromia (Cr_xO_y), and metals, such as Pt-based compositions.[4,13] During the last years, the interest in Pt-based catalysts has been caused by the significant health issues derived from possible chromium spilling or exposure, as well as rapid coking and sintering of chromia-based materials.[14−16] Nevertheless, Pt-based catalysts can undergo rapid deactivation due to coke formation and sintering at high temperatures, which requires implementing regeneration processes.[17] A possible way to overcome the problem of coke formation is the formulation of new and more efficient catalysts, as well as to optimize reaction conditions, such as temperature, pressure, and gas feed composition.[16]

Several studies provide insight into the PDH reaction at the atomic level within the framework of the DFT modeling.[12,13,18−24] These studies indicate that the rate-limiting process of PDH by Pt catalysts is the adsorption of propane followed by the first activation of a C−H bond to give adsorbed propyl intermediate.[12,13,20,25] Calculations have also characterized competitive side reactions such as deep dehydrogenation and C−C bond breaking and compared them with productive propene formation.[23] Recently, DFT-based kinetic Monte Carlo (KMC) simulations revealed that in the initial stage of PDH, there is a quick deactivation of the active sites in the metal surface, where C_2/C_1 carbon species are tightly adsorbed.[12] These C_2/C_1 species formed at the early deactivation stage are proposed to be the precursor of coke formation.[12] There is no consensus in the bibliography about the topology of the active site of Pt catalyst for PDH. Nevertheless, Fricke et al. have recently combined DFT calculations with Bayesian statistics and reported experimental literature, concluding that Pt(211) is the dominant active facet and is more selective toward propene than Pt(111) and Pt(100).[26] In the same line, if we compare the energy barriers for the first C−H activation of propane on different Pt surface topologies, we observe the following reactivity trend: Pt(111) < Pt(100) < Pt(211).[23,24] Also, Zhu et al. have computationally compared Pt(211) and Pt(111) facets, concluding that the activity on Pt(211) is orders of magnitude greater than on Pt(111), while its selectivity depends on the reaction conditions.[27] Despite all these achievements, the application of DFT methods in the discovery of heterogeneous catalysts in processes such as PDH encounters important issues due to the high degree of complexity of such materials, whose catalytic properties are usually modulated by interfacial effects, particle size, speciation, feed composition, temperature, and pressure. Large-scale models enabling the study of catalytic systems of thousands of atoms and dynamic properties are required to exploit the potential of high-performance computers in the *in silico* discovery of catalytic materials. Current methodologies can hardly address such complexity and require new computational strategies that allow one to operate beyond the atomistic level and with an accuracy close to that of DFT-based methods.

During the last years, reactive Molecular Dynamics (MD) approaches based on force fields, such as ReaxFF,[28−31] COMB,[32−34] or AIREBO,[35] have gained significant attention due to their ability to reproduce chemical reactions, including bond-breaking and bond formation (as *ab initio* Molecular Dynamics, AIMD) for large systems. The ReaxFF developed by van Duin in 2001,[28−31] uses the so-called bond order (BO) formalism, which is a general relation between bond length and bond order, and further bond order and bond energy, leading to proper bond dissociation/formation energies. The ReaxFF approach has demonstrated significant potential in diverse fields, including investigations of catalyzed reactions,[36−40] conformational dynamics of biomolecules,[41] oxidation of metal surfaces,[42] and other applications.[29,43,44] Accurate reactive ReaxFF calculations require the assessment of the transferability of existing force-field parameters and, in many cases, the development of specific force-field parameters for the target catalytic process. In the development process, one must generate either computational or experimental reference data for training and validation sets. This process may benefit from the existing DFT literature on the reaction mechanism of PDH catalyzed by Pt,[26] although often, computational open data do not contain all necessary information, and performing new calculations is necessary.

This work aims to develop a reactive ReaxFF force field to study the PDH reaction on Pt catalysts. The general procedure for the ReaxFF force-field development is depicted in Scheme 1. Initially, the transferability of existing parameters has to be assessed by comparing them with reference data, for example, a previous computational study on the mechanism of PDH on the Pt(111) surface.[13] In this case, the force field required reparametrization and generation of a new training set based on DFT calculations on selected reaction intermediates and energy profiles for key C−H and C−C bonds breaking. The commercially available Covariance Matrix Adaptation-Evolution Strategy (CMA-ES) method was employed to optimize the parameter of the ReaxFF force field.

We validated the newly generated ReaxFF force field internally and externally by performing static calculations and reactive dynamic simulations. Moreover, simulations on surfaces of different topologies and temperatures allowed us to gain insight into the PDH mechanism occurring on Pt surfaces.

https://doi.org/10.1021/acs.jpcc.3c07126
J. Phys. Chem. C 2024, 128, 2844−2855

Scheme 1. General Workflow for ReaxFF Force-Field Development

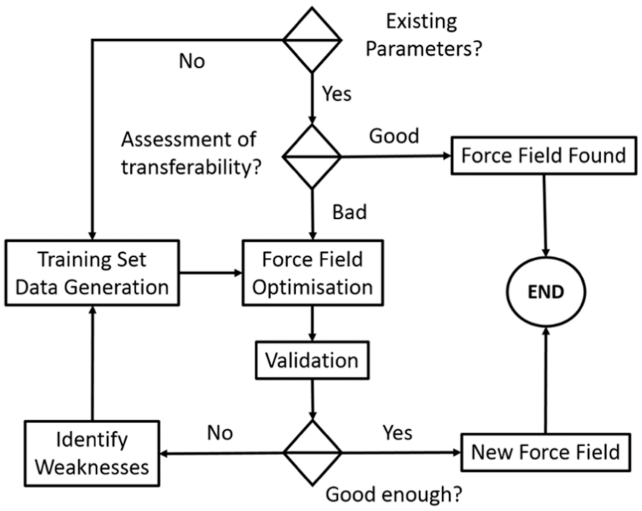

METHODS

DFT Calculations. The training data to develop the ReaxFF force-field parameters was generated from density functional theory (DFT) calculations. Vienna ab initio simulation package (VASP 5.3.5)[45−48] was selected to perform DFT calculations, using the revised-PBE (RPBE-GGA) functional and projector augmented wave (PAW) pseudopotentials.[49,50] The plane-wave basis set corresponded to $2s^2 2p^2$, $1s^1$, and $5d^9 6s^1$ valence electrons of C, H, and Pt atoms, respectively. The cutoff energy for the plane-waves basis set was set as 400 eV. The Monkhorst−Pack[51] 3 × 3 × 1 *k*-point mesh was used for the integration in the reciprocal space. The convergence criterion for the electronic minimization was set at 10^{-7} eV, with the forces over all atoms being smaller than 0.03 eV $Å^{-1}$. The partial occupancies of the orbitals were established using the Methfessel-Paxton scheme[52] with a smearing of 0.2 eV. The Pt(111) surface used in the DFT training set was modeled as a p(3 × 3) 5-layer Pt slab, with a unit cell of 8.44 × 8.44 × 22.17 $Å^3$. A data set collection of the structures used to build the training set is available in the ioChem-BD repository[53] (freely accessible online: 10.19061/iochem-bd-2-66).

ReaxFF Method. The ReaxFF[28] interatomic potential was designed to simulate reactive events through a bond order concept. This concept, developed by Abell,[54] Tersoff,[55,56] and Brenner,[57] allows to calculate the bond order empirically at each simulation step from the interatomic distances. Numerically, the ReaxFF potential energy of the system is defined as the sum of different energy contributions:

$$E_{system} = E_{bond} + E_{over} + E_{angle} + E_{tors} + E_{vdWaals} + E_{Coulomb} + E_{specific} \quad (1)$$

The first four terms stand for the covalent contributions and represent the bonding energy between two atoms (E_{bond}), an energy penalty to prevent the over coordination of atoms (E_{over}), the three-body angle strain energy (E_{angle}), and the four-body dihedral strain energy (E_{tors}). $E_{vdWaals}$ and $E_{Coulomb}$ are the nonbonded interactions representing the dispersive and electrostatic contributions calculated over all the atoms regardless of connectivity and bond order. The last term ($E_{specific}$) is related to some specific energy contributions, calculated only in special cases, such as lone pair energy, conjugation, or hydrogen binding. All of the covalent terms in eq 1 are bond-order-dependent, and since the bond orders are calculated in each step, the bonds can break or form during the simulation. The short-range interactions for the van der Waals energy are described by a distance-corrected Morse potential. The Coulomb energy is calculated by the electronegativity equalization method (EEM).[29,30,33,58,59]

ReaxFF Calculations. The relative energies of the intermediates and the energy profiles were obtained by static ReaxFF calculations, which have been performed using the parameter estimation L-BFGS algorithm (Limited Memory Broyden−Fletcher−Goldfarb−Shanno algorithm)[60] with a maximum number of iterations of 10,000 and with a force convergence criterion of 4.2 kJ mol^{-1} $Å^{-1}$. ReaxFF MD simulations were performed at constant temperature (NVT) with a Berendsen thermostat[61] and a damping constant of 100 fs. The Velocity-Verlet integration method was employed to calculate the trajectories of the particles during MD simulations. The simulation time of MD simulations for productive runs was set to 2 ns, and the time step used was 0.25 fs, which is the default value in the ReaxFF implementation. This was preceded by an initial equilibration at 300 K for 50 ps and heating to working temperature for 50 ps.

Optimizer of Force-Field Parameters. The force-field parameters were optimized against DFT data using the Covariance Matrix Adaptation Evolution Strategy (CMA-ES)[62−65] as implemented in the 2020.103 version of the Amsterdam Modeling Suite (AMS) package of programs. Since CMA-ES is a stochastic method, each force-field optimization has been performed 5 times to ensure that the minimization of the error function is close enough to a global minimum. The number of iterations was set to 10,000 for each run with a sample size of 60, bringing the total number of error function evaluations to 600,000.

RESULTS AND DISCUSSION

Development of Pt/C/H Force-Field Parameters. To obtain ReaxFF Pt/C/H force-field parameters for describing the PDH reaction catalyzed by Pt, we retrained a previous set of atomic and interatomic parameters developed to study the interaction between platinum clusters and carbon platelets.[66] This force field exhibits an appropriate description of Pt, C, and H atomic parameters, as well as Pt−Pt, Pt−C, and Pt−H interactions and C−H bonding. However, its assessment revealed that these parameters were unable to reproduce the thermodynamics and kinetics of reactive events involving C−H and C−C activations. Note that other ReaxFF Pt/C/H force-field parameters were also developed such as those for describing the adsorption of small C/H molecules (e.g., H, C, CH, CH_2, CH_3) on Pt clusters.[67,68] Still, they are not suitable for describing reactive events in hydrocarbons. Thus, the retraining of Pt/C/H force field[66] aims to balance the Pt−C/H interactions in physisorbed species (*e.g.*, propane) and chemisorbed (e.g., propyl) and to describe C−H, C−C, and H−H bond-breaking/forming processes on the platinum surface. Table S1 lists the retrained force-field parameters.

DFT calculations were used to build a training set, including geometries, adsorption energies of various species, relative energies of reaction intermediates, and energy scans of key elementary steps of the PDH mechanism. As a reference for

https://doi.org/10.1021/acs.jpcc.3c07126
J. Phys. Chem. C 2024, 128, 2844−2855

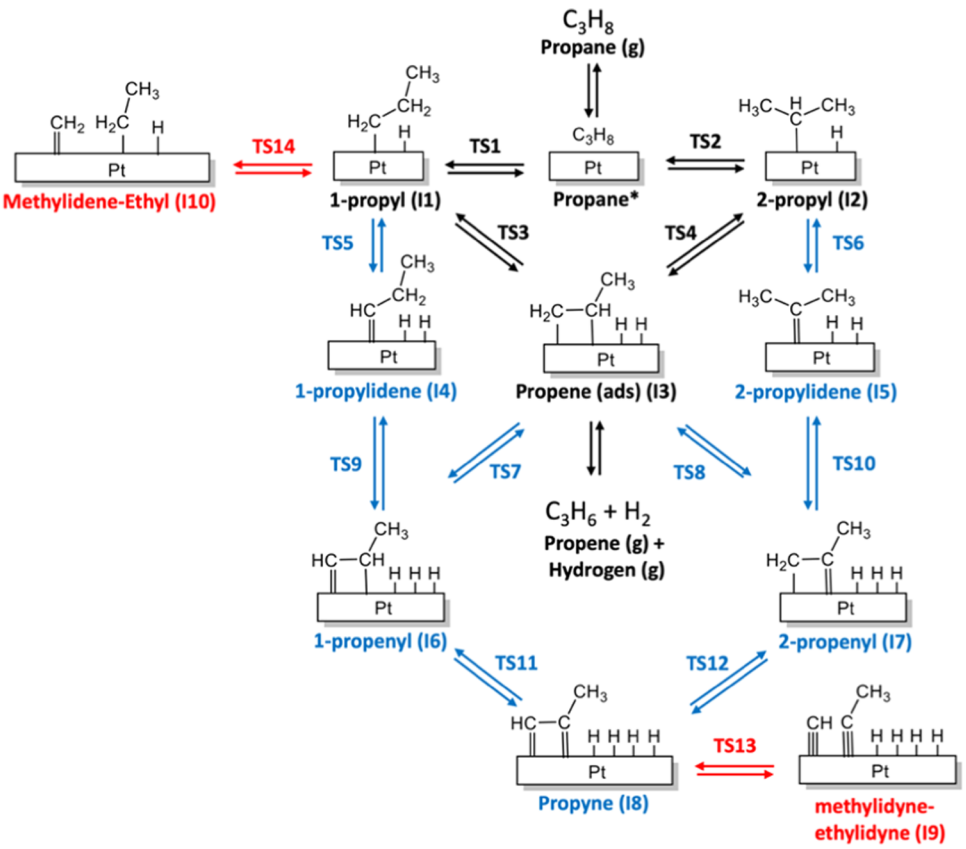

Figure 2. Simplified representation of reaction network for PDH over Pt catalysts proposed by Saerens et al.,[13] used for building the training set. The main production pathways are colored in black, deep dehydrogenation pathways in blue, and C−C bond-cracking pathways in red.

the training set, we choose the reaction mechanism proposed by Saerens et al.[13] based on DFT calculations performed on the Pt(111) slab. Figure 2 shows a simplified reaction network during the PDH process over Pt catalysts; the black arrows point out the pathways for propene formation, while the blue and red arrows denote deep dehydrogenation and C−C bond-cracking side reactions, respectively. These later elementary reactions can form different adsorbed intermediates, such as 1-, 2-propenyl, methylidyne, and ethylidyne (see Figure 2), which are considered the precursors of coke formation. Thus, our training set contains the geometries and relative energies of the intermediates depicted in Figure 2, as well as the adsorption energies of propane and propene. For propene, the training set specifically includes the desorption process scan, employing both energy and structure differences derived from DFT calculations. We expect these data to be crucial for ReaxFF simulations because desorption of propene to the gas phase is the entropic driving force for the PDH reaction. Finally, we calculated the energy and the geometry variations of key elementary steps associated with C−H and C−C bond-breaking/forming processes. These scans include first C−H activation at primary and secondary propane carbons on the Pt(111) surface (**TS1** and **TS2** in Figure 2), the corresponding second C−H activation to give the adsorbed propene (**TS3** and **TS4**), further C−H activation at adsorbed propene to give 1-propenyl intermediate (**TS7**, deep dehydrogenation), and of C−C bond-breaking processes at the early and the late stages of the reaction (**TS13** and **TS14** in Figure 2). Note that in the force-field reparameterization, we did not employ the algorithms for transition state search in DFT and ReaxFF, but energy scans of the reaction coordinate. The selection of this procedure is based on two main reasons: (1) the ReaxFF parameters at the beginning of the development are poor and cannot guarantee obtaining the transition state structure;[69] (2) the energy scans give a smooth energy evolution along the reaction coordinate advance, ensuring in most cases a single energy maximum around the transition state geometry. Table 1 summarizes the training set used in force-field development, which consists of 95 energies, 1236 distances, 3439 angles, and 9595 dihedrals, resulting in a total of 14,365 entries for the

Table 1. Summary of the Training Set Used for the Parametrization of the Pt/C/H Force Field

process	specification	entries
relative energies	1-propyl (**I1**), 2-propyl (**I2**), propene (**I3**), 1-propylidene (**I4**), 2-propylidene (**I5**), 1-propenyl (**I6**), 2-propenyl (**I7**), propyne (**I8**), methylidyne ethylidyne (**I9**)	1092
adsorption energy	C_3H_8*, C_3H_6*	178
desorption process	propene	556
C−H activation	$CH_3CH_2CH_3$* → $CH_3CH_2CH_2$* + H* (**TS1**) $CH_3CH_2CH_3$* → CH_3CHCH_3* + H* (**TS2**) $CH_3CH_2CH_2$* + H* → CH_3CHCH_2* + 2H* (**TS3**) CH_3CHCH_3* + H* → CH_3CHCH_2* + 2H* (**TS4**) CH_3CHCH_2* + 2H* → CH_3CHCH* + 3H* (**TS7**)	5733
C−C activation	CH_3CCH* + 4H* → CH_3C* + CH* + 4H* (**TS13**) $CH_3CH_2CH_2$* + H* → CH_3CH_2* + CH_2* + H* (**TS14**)	6806

https://doi.org/10.1021/acs.jpcc.3c07126
J. Phys. Chem. C 2024, 128, 2844−2855

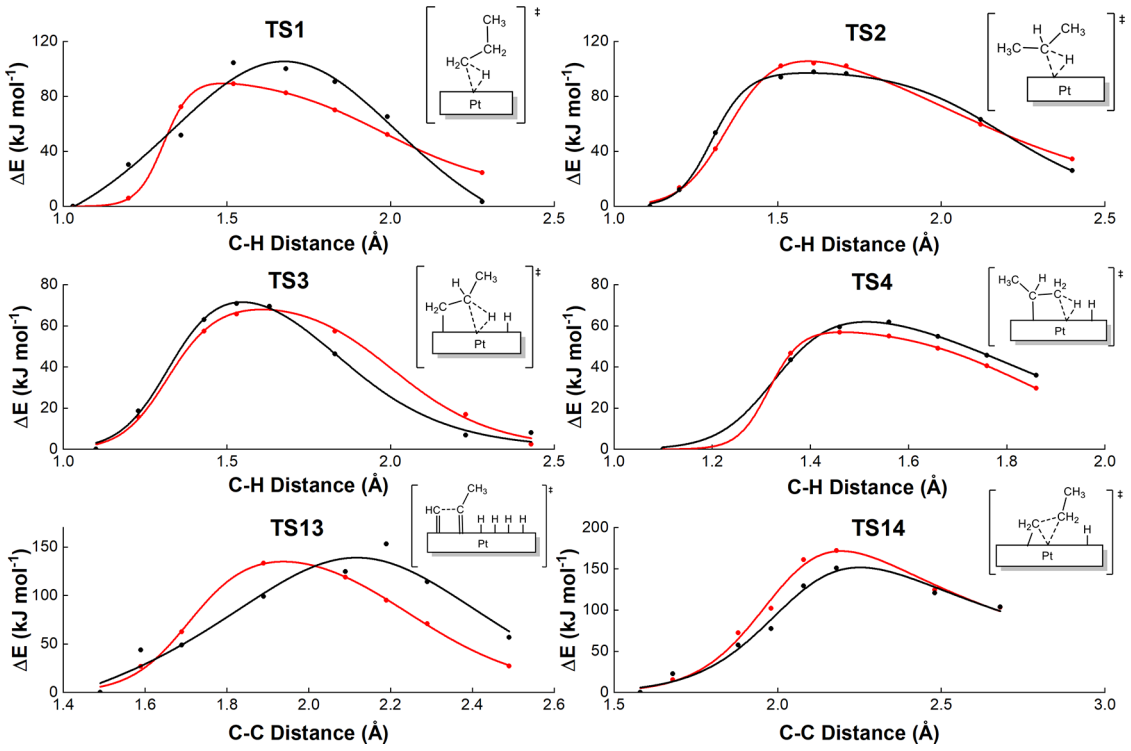

Figure 3. Comparison of ReaxFF and DFT energy scans of four C−H bond activations (**TS1**, **TS2**, **TS3**, and **TS4**) and two C−C bond activations (**TS13** and **TS14**). Black and red lines correspond to ReaxFF and DFT calculations, respectively. Energies are in kJ mol^{-1} and distances in Å.

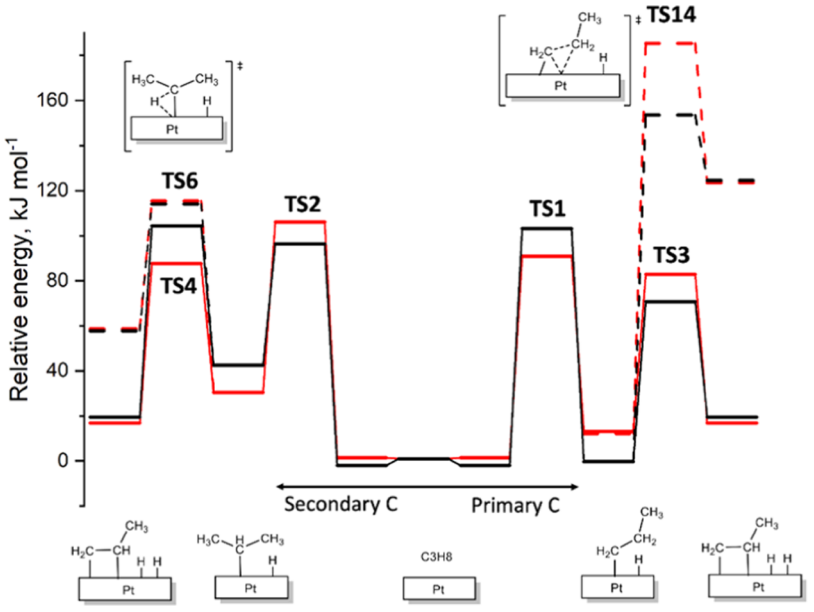

Figure 4. Comparison of ReaxFF and DFT energy profile (kJ mol^{-1}) for propane dehydrogenation reaction on Pt(111) surface starting by a C−H activation at primary carbon (right) and at secondary carbon (left). Black and red lines correspond to ReaxFF and DFT calculations, respectively, while dashed lines correspond to side reactions.

fitting. As detailed in the Methods section, the ReaxFF force field was fitted using the CMA-ES method, which has led to the new **2023-Pt/C/H** ReaxFF force field, whose parameters are listed in the Supporting Information.

Validation of 2023-Pt/C/H Force Field. The computed DFT geometries and energies used in the parametrization process were employed to internally validate the **2023-Pt/C/H** force field. The relative energies of PDH reaction intermediates over Pt(111) calculated using the developed force field compare well with the DFT energies (Table S2), giving a mean absolute error (MAE) of 14.2 kJ mol^{-1}. ReaxFF portrays the right trend for the adsorption energies of propane and propene that are computed to be isoenergetic and exothermic, respectively (+0.4 kJ mol^{-1} versus −2.9 kJ mol^{-1}, and −56.9 kJ mol^{-1} versus −66.5 kJ mol^{-1}, for DFT and ReaxFF, respectively). The other chemical trends are also well reproduced by the **2023-Pt/C/H** force field compared to DFT data: (1) the propane C−H bond breaking of the primary

https://doi.org/10.1021/acs.jpcc.3c07126
J. Phys. Chem. C 2024, 128, 2844−2855

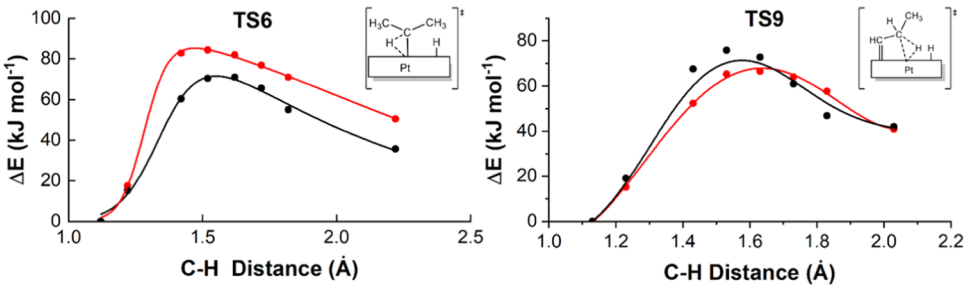

Figure 5. Comparison of ReaxFF and DFT energy scans of two externally validated C−H bond activations (**TS6** and **TS9**). Black and red lines correspond to ReaxFF and DFT calculations, respectively. Energies in kJ mol^{-1} and distances in Å.

Table 2. Comparison of ReaxFF and DFT Energies of the C−H and C−C Bond-Breaking Processes on Different Pt Topologies[a]

		$\Delta\Delta E^{\ddagger}$	$\Delta\Delta E^{\ddagger}$ (DFT)[b,c]		$\Delta\Delta E^{\ddagger}$ (ReaxFF)	
elementary reactions		Pt(111)	Pt(100)	Pt(211)	Pt(100)	Pt(211)
$CH_3CH_2CH_3^* \rightarrow CH_3CH_2CH_2^* + H^*$	**TS1**	0.0	−25.0	−35.6	−16.3	−26.8
$CH_3CH_2CH_3^* \rightarrow CH_3CHCH_3^* + H^*$	**TS2**	0.0	−26.8	−40.2	−19.3	−33.0
$CH_3CH_2CH_2^* \rightarrow CH_3CHCH_2^* + H^*$	**TS3**	0.0	−29.7	−51.0	−15.1	−26.8
$CH_3CHCH_3^* \rightarrow CH_3CHCH_2^* + H^*$	**TS4**	0.0	−28.0	−33.1	−3.3	−28.0
$CH_3CH_2CH_2^* \rightarrow CH_3CH_2^* + CH_2^*$	**TS14**	0.0	−50.2	−59.0	−59.4	−65.3

[a]Energy barriers (kJ mol^{-1}) for Pt(100) and Pt(211) are given as relative energies, with Pt(111) used as reference. The negative values denote a lowering of the energy barriers. [b]Values taken from ref 23. [c]Values taken from ref 24.

carbon (**I1**) is thermodynamically favored over the secondary carbon (**I2**); (2) from the propyl intermediates (**I1** and **I2**), formation of the adsorbed alkene (**I3**) is preferred over the formation of propylidene intermediates (**I4** and **I5**); (3) from adsorbed propene, C_3H_6*, deep dehydrogenation is energetically favored with respect to the desorption, but the entropic term at high temperatures can invert this trend; and (4) the adsorbed propyne is more likely to reversely hydrogenate than to further evolve to C−C bond-breaking species.

Figure 3 compares the ReaxFF and DFT results of the energy scan for representative C−H and C−C bond activation over the Pt(111) surface to assess whether the developed force field correctly describes the reaction kinetics. Table S2 lists the estimated energy barriers from these curves derived from ReaxFF and DFT calculations. Although transition state searches can be performed using both ReaxFF and DFT, we fitted these curves to ensure that the ReaxFF energy evolves smoothly with the bond distances; in other words, there are no energy jumps, which could interfere with reaction kinetics. In all cases, the energy and bond distance curves from ReaxFF match well with those from DFT in both value and trend. The MAE for the estimated energy barriers (11.5 kJ mol^{-1}) is of the same order as that measured for the relative energies of the reaction intermediates (14.2 kJ mol^{-1}, see above).

As illustrated in Figure 4, which compares the ReaxFF and DFT reaction energy profiles, the **2023-Pt/C/H** force-field parameters reproduce the key trends: (1) the energy barrier for C−C bond breaking is higher than those for C−H activation, and (2) the first C−H bond activations (105 and 98 kJ mol^{-1} for primary (**TS1**) and secondary (**TS2**) carbons, respectively) have higher energy cost than the second C−H bond activation from propyl intermediates (71 and 62 kJ mol^{-1} from 1- (**TS3**) and 2-propyl (**TS4**) intermediates, respectively). This latter trend agrees with previous mechanistic studies indicating that the rate-determining step for the PDH reaction is the first C−H bond activation of propane.[23] The DFT energy barrier for C−H activation at primary carbons is only slightly lower (15 kJ mol^{-1}) than that at secondary carbons, and ReaxFF inverts this trend in a small extent (see Table S3). Nevertheless, reactive MD simulations (see below) show that PDH proceeds preferentially through the primary C−H activation pathway, due to the statistical prevalence of primary C−H bonds over secondary ones (3:1), and the thermodynamically disfavored formation of 2-propyl intermediate resulting from secondary C−H bond activation.

We also performed an external validation of **2023-Pt/C/H** force-field parameters by evaluating the energy evolution of two C−H bond activation processes not included in the training set: $CH_3CHCH_3^* + H^* \rightarrow CH_3CCH_3^* + 2H^*$, **TS6**; and $CH_3CH_2CH^* + 2H^* \rightarrow CH_3CHCH^* + 3H^*$, **TS9** (see Figure 2). The ReaxFF calculations reproduce DFT results well (see Figure 5), the absolute errors being 13.4 and 9.2 kJ mol^{-1} for **TS6** and **TS9** elementary reactions, respectively. These errors are similar to those of the MAE (11.5 kJ mol^{-1}) determined during internal validation by evaluating the energy barriers of the elementary reaction steps included in the training set.

To further validate externally the **2023-Pt/C/H** force field, we have evaluated the energy barriers for selected C−H bond (**TS1**, **TS2**, **TS3**, and **TS4**) and C−C bond (**TS14**) activations over different types of the platinum surfaces, Pt(111), Pt(100) and Pt(211). Then, we compared them with reported DFT values.[23,24] Since, in this case, we aim to assess trends rather than values, we compared the variations of the energy barriers on moving from Pt(111) to Pt(100) and Pt(211) surfaces (values reported in Table 2). As a general trend, all the computed energy barriers over Pt(100) and Pt(211), containing low-coordinated Pt atoms, are lower than those on the Pt(111) surface, and this trend is more pronounced for the stepped Pt(211). In line with these trends, the ReaxFF relative energy barriers for the Pt(100) surface are all negative and have even larger negative values for the Pt(211) surface. Thus, the validation of the **2023-Pt/C/H** force field indicates that it is not only able to describe the main features of propane

https://doi.org/10.1021/acs.jpcc.3c07126
J. Phys. Chem. C 2024, 128, 2844−2855

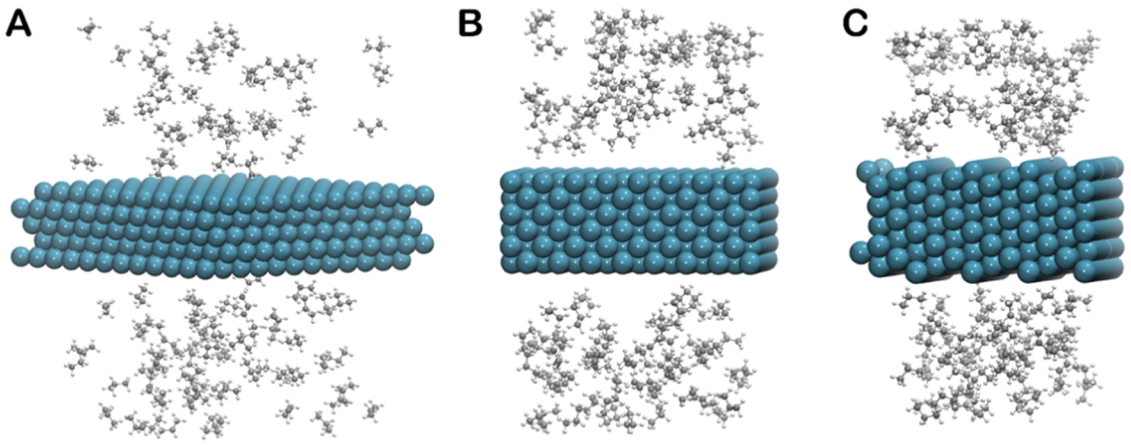

Figure 6. Initial configurations of selected systems to simulate PDH with ReaxFF reactive MD using the **2023-Pt/C/H** force field: (A) Pt(111) surface, (B) Pt(100) surface, (C) Pt(211) surface.

Table 3. Comparison of DFT, Relative Energy Barriers for the C−H Activation of Propane ($\Delta\Delta E_{C-H}^{\ddagger}$, in kJ mol^{-1}) with Relative Rates of ReaxFF Reactive MD Simulations of Propane Molecules on Pt(111), Pt(100), and Pt(211) Surfaces[a]

			average product distribution			
surface	$\Delta\Delta E_{C-H}^{\ddagger}$ (DFT)[b]	relative rate (ReaxFF MD)	reacted[c]	C_3 (propene)	C_2	C_1
Pt(111)	0.0	1.00	4.2 ± 0.1	1.4 (0.4)	2.8	2.8
Pt(100)	−25.1	1.21	5.2 ± 0.1	1.8 (0.6)	2.2	5.8
Pt(211)	−35.6	1.40	6.0 ± 0.3	1.8 (1.4)	2.8	7.0

[a]Average product distribution (reacted propane molecules and C_3, C_2, and C_1 hydrocarbon species) after five simulation runs of 2 ns each. [b]Values taken from refs 23 and 24. [c]Uncertainty estimation by comparing the average values derived from the two largest ensembles, $N = 4$ and $N = 5$ simulation runs.

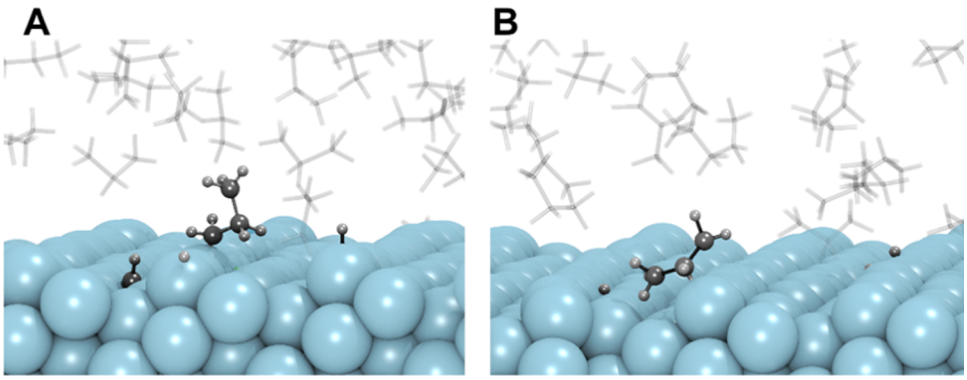

Figure 7. Illustrative snapshots of the formation of 1-propyl (A) and 2-propyl (B) intermediates on the step sites of the Pt(211) surface during the ReaxFF simulation.

dehydrogenation over Pt(111) but also to gauge the effects of Pt topology on the reaction, enabling the study of different types of Pt catalysts. The ability of the **2023-Pt/C/H** force field to describe the propane reactivity on Pt surfaces with different topologies is further analyzed in the next section.

ReaxFF Molecular Dynamic Simulations of Propane Reactivity on the Pt(111), Pt(100), and Pt(211) Surfaces. The newly developed ReaxFF **2023-Pt/C/H** force field was used to compare the reactivity of propane on Pt surfaces with different topologies via reactive molecular dynamics (MD) simulations. The selected surfaces are Pt(111), Pt(100), and the stepped Pt(211), and the corresponding simulated systems are shown in Figure 6. The model for the Pt(111) surface was composed of a five-layered p(8 × 8) supercell with box parameters of 29.3 × 33.8 × 51.5 Å^3, the model for Pt(100) surface was formed by a p(8 × 9) supercell with six layers and a 31.8 × 35.8 × 54.8 Å^3 box, and the model for Pt(211) surface was composed of a six-layer p(12 × 6) supercell in a box of 45.0 × 27.5 × 51.5 Å^3. The space between the periodic slabs was 42.0 Å. The dimensions of the Pt models were selected to ensure that the total number of surface Pt atoms is the same for three scenarios (288 for each system), allowing a straightforward comparison of the simulation outcomes. The propane molecules were randomly distributed in the empty space of the simulation box. Initially, we built a system mimicking the experimental working pressures for propane (1−2 bar), but no reaction was observed within the available simulation time (nanoscale). Since our main goal is to evaluate the performance of the **2023-Pt/C/H** force field on different Pt topologies, we increased the number of propane molecules in the simulation box up to 100 to observe reactive events. We ran 5 independent simulations of 2 ns for each, and the results

https://doi.org/10.1021/acs.jpcc.3c07126
J. Phys. Chem. C 2024, 128, 2844−2855

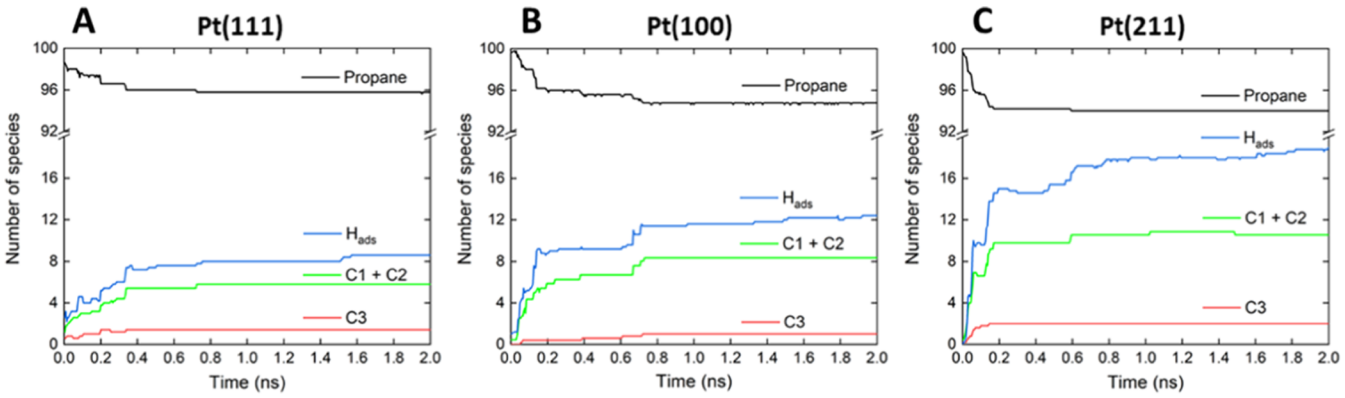

Figure 8. Evolution of the average number of species during the 5 simulation runs of 2 ns for systems defined in Figure 6, Pt(111) facet (A), Pt(100) facet (B), and Pt(211) facet (C).

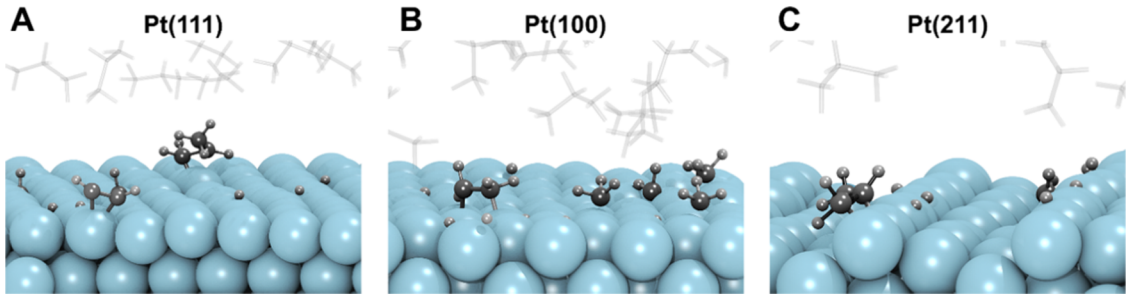

Figure 9. Illustrative snapshots of the formation of deep dehydrogenated and cracked species on Pt(111) (A), Pt(100) (B), and Pt(211) (C) surfaces during ReaxFF simulations.

were averaged over the 5 runs. Before the production runs, the systems were equilibrated as described in the Methods section. To compare the different surfaces, the ReaxFF MD simulations were performed at 873 K, and then, the effect of the temperature was studied on the Pt(111) system.

Table 3 compares the relative, DFT-computed energy barriers for the initial C−H activation of propane previously reported in the bibliography,[23,24] with the relative, ReaxFF reaction rates, which are defined as the fraction of reacted propane molecules at the end of the simulation averaged over the five runs and normalized respect to the value for Pt(111) surface. ReaxFF simulations predict the following PDH reactivity order as a function of Pt surface topology: Pt(111) < Pt(100) < Pt(211). This trend correlates with the DFT-computed energy barriers for the initial C−H activation in propane, which has been used as an indicator to evaluate the activity variation on different types of surfaces and catalysts.[19,70−72] We observed that the reaction is initiated by C−H activation, on either the primary or secondary carbon of propane (**TS1** and **TS2** pathways, respectively, in Figure 2). Then, the 1- or the 2-propyl intermediates undergo a second C−H activation to form the adsorbed propene, which can desorb or further react to give deep dehydrogenated or cracked products. The C−H bond activation and other reactions occur at the step sites for the more reactive stepped Pt(211) surface. This agrees with previous DFT studies, which indicated that step sites play a crucial role in propane activation, explaining the kinetic preference with respect to flat surfaces.[23] Figure 7 depicts representative snapshots of the reactive dynamic simulation of propene formation on the Pt(211) surface. Also, ReaxFF simulations showed that the adsorbed hydrogen atoms, generated from propane dehydrogenation, diffuse on the platinum surfaces, reacting to form H_2 molecules, which then desorb.

Figure 8 compares the evolution of different species during the propane dehydrogenation simulation on the three different platinum surface models considered. Interestingly, for all of the surfaces, the propane conversion rate drops significantly before the end of the simulation. We theorize that platinum site occupancies become relevant as the percentage of free sites decreases. In other words, the deep dehydrogenation and the cracking generate H, C_1, and C_2 hydrocarbon, adsorbed species that deactivate the platinum surface, blocking the reaction of further propane molecules. In addition, these C_1 and C_2 species can be seen as precursors of observed coke formation. This is in line with recent kinetic Monte Carlo simulations, which indicated that in the initial stages of the reaction, there is a quick deactivation in the metal surface, where C_1 and C_2 hydrocarbon species are strongly adsorbed.[12] In our simulations, the fast formation of coke precursors is likely to result from the high density of propane reactant molecules required to observe reactive events within the available times. Figure 9 shows representative snapshots of the ReaxFF simulations illustrating the adsorption of hydrogen and hydrocarbons on different surfaces. We observed the formation of different deep dehydrogenated C_3 species such as allyl*, 1-propenyl*, or propyne*, and also of other cracked C_2 and C_1 species such as C_2H_5*, C_2H_4*, and CH_3*. The reactivity order for deep dehydrogenation and cracking as a function of Pt surface topology follows the same trend as the PDH reaction: Pt(111) < Pt(100) < Pt(211); see Table 3 and Figure 8. At the end of our simulations, we estimated that the percentages of Pt atoms on the surface affected by adsorbed species (first and second interaction spheres) are 26.2, 36.6, and 49.4% for Pt(111),

https://doi.org/10.1021/acs.jpcc.3c07126
J. Phys. Chem. C 2024, 128, 2844−2855

Pt(100), and Pt(211), respectively. The selectivity to propene for the different surfaces can be estimated as the ratio between the number of formed propene molecules and the number of propane molecules transformed into C_2 and C_1 species via cracking and deep dehydrogenation. In these simulations, the C_3 deep dehydrogenated species are statistically irrelevant. From the data in Table 3, we find that Pt(211) is the most selective of the surfaces, followed by Pt(100) and Pt(111). The calculated selectivities are relatively low (ranging from 13 to 25%), probably due to the artificially high propane concentration required for our simulations. Nevertheless, we were able to predict the Pt(211) facet as the more selective, in agreement with a recent study, in which six kinetic models were validated using data from different DFT functionals and experiments.[26]

To evaluate the ability of the ReaxFF force field to reproduce the temperature-dependent behavior of the Pt catalyst, simulations of propane dehydrogenation were also conducted on a Pt(111) surface at different temperatures (773, 873, 973, and 1073 K). The results of the simulations are summarized in Table 4 and Figure 10. Propane conversion

Table 4. ReaxFF Reactive MD Simulations of Propane Molecules on the Pt(111) Surface at Different Temperatures[a]

		average product distribution			
T, K	relative rate (ReaxFF MD)	reacted	C_3 (propene)	C_2	C_1
773	1.0	2.2	1.1 (0.0)	1.0	1.0
873	3.3	4.2	1.4 (0.4)	2.8	2.8
973	8.3	14.8	4.2 (1.4)	9.8	11.6
1073	19.3	27.6	8.2 (2.6)	17.6	23.0

[a]Relative rate and average product distribution of reacted propane molecules (C_3, C_2, and C_1 hydrocarbon species) after 5 simulation runs of 2 ns each.

increases exponentially with increasing temperature and, similarly, the generation of C_2 and C_1 hydrocarbon species adsorbed on the surface. These findings indicate that, although higher temperatures may lead to more efficient propane conversion, it may also result in a more significant amount of coke formation on the platinum surface, subsequently leading to the deactivation of the catalyst.[17]

Reactive simulations at different temperatures can also be used to determine the apparent activation energy of the reaction and compare it with experimental values.[73] To build the Arrhenius plot (Figure 10B), we estimated the rate constants at initial times to avoid the effect of excessive deactivation of the platinum surface due to the high density of propane used in simulations (see discussion above). The concentration of reacted propane was replaced by the number of reacted propane molecules, and the same time interval was considered at each temperature to obtain the initial reaction rate. Initially, we selected the minimal reaction time satisfying the linearity requirements of the Arrhenius plot, the natural logarithm of the reaction rate against the inverse temperature. Using as threshold $r^2 \geq 0.99$, the simulation time of 0.045 ns was initially chosen to build the Arrhenius plot (see Figure S1), providing an apparent activation energy (E_a) of 73 kJ mol^{-1}. The computed average value of E_a along the time interval from 0.045 to 0.120 ns, where all points exhibit linear plots ($r^2 \geq 0.99$), is 68 kJ mol^{-1} with a standard deviation of 3 kJ mol^{-1} (see Table S4). These estimates are in good agreement with the upper value reported for PDH over Pt/Al_2O_3 nanocatalysts, in which the apparent activation energy increases with the size of the Pt catalyst until it reaches 75 kJ mol^{-1} for large nanoparticles of ~5 nm.[74,75]

CONCLUSIONS

In the present work, we have developed the **2023-Pt/C/H** ReaxFF reactive force field for simulating propane dehydrogenation (PDH) on Pt surfaces. The parametrization was performed using a DFT-based training set, including geometries, adsorption and relative energies of the reaction intermediates on Pt(111), and key elementary reaction steps of selected C−H and C−C bond-breaking processes. There is overall good agreement between ReaxFF and DFT results in the internal validation, with mean absolute errors (MAEs) for relative energies of intermediates and energy barriers of 14 and 12 kJ mol^{-1}, respectively. The external validation revealed that the **2023-Pt/C/H** force field not only describes the main reaction features of PDH on the Pt(111) surface but also can gauge the effects of Pt topology on the reaction, enabling the study of different types of Pt catalysts.

To further test the developed force field and get insight into the reactivity of propane on Pt surfaces with different topologies, we performed reactive MD simulations on

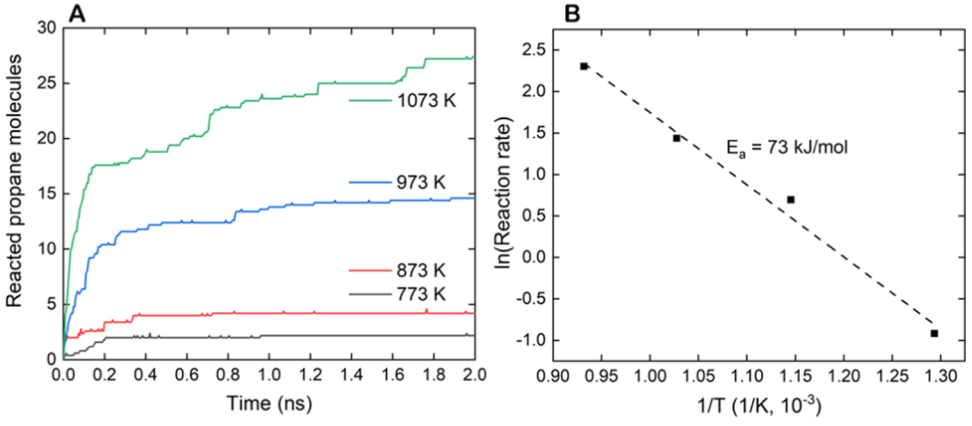

Figure 10. Evolution of the average number of species during the five simulation runs of 2 ns on the Pt(111) facet at different temperatures (A) and the Arrhenius plot derived from simulations (B).

https://doi.org/10.1021/acs.jpcc.3c07126
J. Phys. Chem. C 2024, 128, 2844−2855

Pt(111), Pt(100), and Pt(211) surfaces and also at different temperatures for Pt(111). ReaxFF simulations on large-scale systems at experimental temperatures predict the following reactivity order: Pt(111) < Pt(100) < Pt(211). In the most reactive Pt(211) surface, the propane activation is exclusively observed on low-coordinated Pt atoms at the steps, which are crucial to enhance catalytic activity. Simulations show quick deactivation in the platinum surface, where H, C_1, and C_2 hydrocarbon species, formed from deep dehydrogenation and the C−C cracking side reactions, are strongly adsorbed. These C_1 and C_2 species can be precursors of the experimentally observed coke formation, poisoning the catalyst and reducing selectivity toward propene formation. The measured selectivity as a function of surface topology follows the order Pt(211) > Pt(100) > Pt(111). Simulations at different temperatures on the Pt(111) surface allowed building Arrhenius plots to determine computationally the apparent activation energy, 73 kJ mol^{-1}, which is close to that determined experimentally for large nanoparticles (∼5 nm) supported on alumina (75 kJ mol^{-1}).

All in all, the **2023-Pt/C/H** ReaxFF reactive force field can be employed to study propane dehydrogenation and its side reactions on different Pt catalysts, including simulations of collective effects such as temperature, propane pressure, and H surface coverage. This will enable analyzing more complex Pt systems under different conditions, driving research toward designing more efficient catalytic processes.

■ ASSOCIATED CONTENT

Supporting Information

The Supporting Information is available free of charge at https://pubs.acs.org/doi/10.1021/acs.jpcc.3c07126.

Additional details of force-field development and validation, **2023-Pt/C/H** ReaxFF reactive force-field parameters, DFT data of the training set through the open-access repository ioChem-BD, and the files "geo" and "trainingset" used as input in AMS optimization of ReaxFF parameters (PDF)

Information on the training set that can be used to re-train the ReaxFF force field (TXT)

Information on the geo set that can be used to re-train the ReaxFF force field (TXT)

■ AUTHOR INFORMATION

Corresponding Authors

Daniel Curulla-Ferré − *TotalEnergies OneTech Belgium, 7181 Seneffe, Belgium*; Email: daniel.curulla-ferre@totalenergies.com

Josep M. Ricart − *Departament de Química Física i Inorgànica, Universitat Rovira i Virgili, 43007 Tarragona, Spain*; Email: josep.ricart@urv.cat

Jorge J. Carbó − *Departament de Química Física i Inorgànica, Universitat Rovira i Virgili, 43007 Tarragona, Spain*; orcid.org/0000-0002-3945-6721; Email: j.carbo@urv.cat

Authors

Antoni Salom-Català − *Departament de Química Física i Inorgànica, Universitat Rovira i Virgili, 43007 Tarragona, Spain*

Evgenii Strugovshchikov − *Departament de Química Física i Inorgànica, Universitat Rovira i Virgili, 43007 Tarragona, Spain*

Kamila Kaźmierczak − *TotalEnergies OneTech Belgium, 7181 Seneffe, Belgium*

Complete contact information is available at: https://pubs.acs.org/10.1021/acs.jpcc.3c07126

Author Contributions

§A.S.-C. and E.S. contributed equally to this work. J.J.C., J.M.R., K.K., and D.C.-F. conceived the initial idea and designed the project. A.S.-C. and E.S. performed force-field optimization, DFT calculations, and ReaxFF simulations. The manuscript was written through the contributions of all authors. All authors have given approval to the final version of the manuscript.

Notes

The authors declare no competing financial interest.

■ ACKNOWLEDGMENTS

This work has been performed as part of Joint Research Agreement between TotalEnergies OneTech Belgium and the Fundació Universitat Rovira i Virgili (Contract Number IPA-6119). J.J.C., J.M.R., A.S.-C., and E.S. thank grant PID2021-128128NB-I00 funded by MINECO/AEI/10.13039/501100011033 and by "ERDF A way of making Europe" and the Generalitat de Catalunya (2021SGR00110).

■ REFERENCES

(1) Liu, M.-J.; Wang, G.; Xu, S.-N.; Zheng, T.-R.; Zhang, Z.-D.; He, S.-B. Reaction Characteristics of Maximizing Light Olefins and Decreasing Methane in C_5 Hydrocarbons Catalytic Pyrolysis. *Pet. Sci.* **2023**, *20* (3), 1909−1921.

(2) Wang, Y.; Yokoi, T.; Tatsumi, T. Selective Production of Light Olefins over Zeolite Catalysts: Impacts of Topology, Acidity, and Particle Size. *Microporous Mesoporous Mater.* **2023**, *358*, No. 112353.

(3) Sekyere, D. T.; Zhang, J.; Chen, Y.; Huang, Y.; Wang, M.; Wang, J.; Niwamanya, N.; Barigye, A.; Tian, Y. Production of Light Olefins and Aromatics via Catalytic Co-Pyrolysis of Biomass and Plastic. *Fuel* **2023**, *333*, No. 126339.

(4) Sattler, J. J. H. B.; Ruiz-Martinez, J.; Santillan-Jimenez, E.; Weckhuysen, B. M. Catalytic Dehydrogenation of Light Alkanes on Metals and Metal Oxides. *Chem. Rev.* **2014**, *114* (20), 10613−10653.

(5) Wang, F.; Xu, Y.; Ren, J.; Li, Y. Experimental Investigation and Modeling of Steam Cracking of Fischer−Tropsch Naphtha for Light Olefins. *Chem. Eng. Process.* **2010**, *49* (1), 51−58.

(6) Kubo, K.; Iida, H.; Namba, S.; Igarashi, A. Ultra-High Steaming Stability of Cu-ZSM-5 Zeolite as Naphtha Cracking Catalyst to Produce Light Olefin. *Catal. Commun.* **2012**, *29*, 162−165.

(7) Nandi, P. G.; Arora, V.; Yasmin, E.; Kumar, A. Pincer-Group and Pincer-Group. Metal Complexes for Catalytic Alkane Dehydrogenation Reactions. In *Pincer-Metal Complexes*; Elsevier, 2022; pp 69−122.

(8) Xu, H.; Cao, M.; Li, Z.; Li, W.; Meng, S.; Song, H. Production of Low Carbon Number Olefins from Natural Gas: Methane-Involved Catalytic Non-Oxidative Propane Dehydrogenation. *Chem. Eng. J.* **2023**, *454*, No. 140508.

(9) Bhasin, M. M.; McCain, J. H.; Vora, B.; Imai, T.; Pujadó, P. R. Dehydrogenation and Oxydehydrogenation of Paraffins to Olefins. *Appl. Catal., A* **2001**, *221* (1−2), 397−419.

(10) Dobis, O.; Benson, S. W. Analysis of Flow Dynamics in a New, Very Low Pressure Reactor. Application to the Reaction: Cl + CH_4 ⇔ HCl + CH_3. *Int. J. Chem. Kinet.* **1987**, *19* (8), 691−708.

(11) Russell, J. J.; Seetula, J. A.; Gutman, D. Kinetics and Thermochemistry of Methyl, Ethyl, and Isopropyl. Study of the

Equilibrium R + HBr ⇔ R-H + Br. *J. Am. Chem. Soc.* **1988**, *110* (10), 3092−3099.
(12) Lian, Z.; Ali, S.; Liu, T.; Si, C.; Li, B.; Su, D. S. Revealing the Janus Character of the Coke Precursor in the Propane Direct Dehydrogenation on Pt Catalysts from a KMC Simulation. *ACS Catal.* **2018**, *8* (5), 4694−4704.
(13) Saerens, S.; Sabbe, M. K.; Galvita, V. V.; Redekop, E. A.; Reyniers, M.-F.; Marin, G. B. The Positive Role of Hydrogen on the Dehydrogenation of Propane on Pt(111). *ACS Catal.* **2017**, *7* (11), 7495−7508.
(14) Davis, R. J.; Griffith, R. H.; Marsh, J. D. F. The Physical Properties of Chromia-Alumina Catalysts. *Adv. Catal.* **1957**, *9*, 155−162.
(15) Tinnemans, S. J.; Kox, M. H. F.; Nijhuis, T. A.; Visser, T.; Weckhuysen, B. M. Real Time Quantitative Raman Spectroscopy of Supported Metal Oxide Catalysts without the Need of an Internal Standard. *Phys. Chem. Chem. Phys.* **2005**, *7* (1), 211.
(16) Liu, G.; Zeng, L.; Zhao, Z.-J.; Tian, H.; Wu, T.; Gong, J. Platinum-Modified ZnO/Al_2O_3 for Propane Dehydrogenation: Minimized Platinum Usage and Improved Catalytic Stability. *ACS Catal.* **2016**, *6* (4), 2158−2162.
(17) Iglesias-Juez, A.; Beale, A. M.; Maaijen, K.; Weng, T. C.; Glatzel, P.; Weckhuysen, B. M. A Combined in Situ Time-Resolved UVVis, Raman and High-Energy Resolution X-Ray Absorption Spectroscopy Study on the Deactivation Behavior of Pt and PtSn Propane Dehydrogenation Catalysts under Industrial Reaction Conditions. *J. Catal.* **2010**, *276* (2), 268−279.
(18) Yang, M.-L.; Zhu, Y.-A.; Fan, C.; Sui, Z.-J.; Chen, D.; Zhou, X.-G. Density Functional Study of the Chemisorption of C_1, C_2 and C_3 Intermediates in Propane Dissociation on Pt(111). *J. Mol. Catal. A* **2010**, *321*, 42−49.
(19) Araujo-Lopez, E.; Vandegehuchte, B. D.; Curulla-Ferré, D.; Sharapa, D. I.; Studt, F. Trends in the Activation of Light Alkanes on Transition-Metal Surfaces. *J. Phys. Chem. C* **2020**, *124* (50), 27503−27510.
(20) Zhu, J.; Yang, M.-L.; Yu, Y.; Zhu, Y.-A.; Sui, Z.-J.; Zhou, X.-G.; Holmen, A.; Chen, D. Size-Dependent Reaction Mechanism and Kinetics for Propane Dehydrogenation over Pt Catalysts. *ACS Catal.* **2015**, *5* (11), 6310−6319.
(21) Valcárcel, A.; Ricart, J. M.; Clotet, A.; Markovits, A.; Minot, C.; Illas, F. Theoretical Study of the Structure of Propene Adsorbed on Pt(111). *Surf. Sci.* **2002**, *519* (3), 250−258.
(22) Valcárcel, A.; Ricart, J. M.; Clotet, A.; Illas, F.; Markovits, A.; Minot, C. Theoretical Study of Dehydrogenation and Isomerisation Reactions of Propylene on Pt(111). *J. Catal.* **2006**, *241* (1), 115−122.
(23) Yang, M.-L.; Zhu, Y.-A.; Fan, C.; Sui, Z.-J.; Chen, D.; Zhou, X.-G. DFT Study of Propane Dehydrogenation on Pt Catalyst: Effects of Step Sites. *Phys. Chem. Chem. Phys.* **2011**, *13* (8), 3257.
(24) Yang, M.-L.; Zhu, J.; Zhu, Y.-A.; Sui, Z.-J.; Yu, Y.-D.; Zhou, X.-G.; Chen, D. Tuning Selectivity and Stability in Propane Dehydrogenation by Shaping Pt Particles: A Combined Experimental and DFT Study. *J. Mol. Catal. A* **2014**, *395*, 329−336.
(25) Caspary, K. J.; Gehrke, H.; Heinritz-Adrian, M.; Schwefer, M.*Handbook of Heterogeneous Catalysis*; Wiley, 2008; pp 3206−3229.
(26) Fricke, C.; Rajbanshi, B.; Walker, E. A.; Terejanu, G.; Heyden, A. Propane Dehydrogenation on Platinum Catalysts: Identifying the Active Sites through Bayesian Analysis. *ACS Catal.* **2022**, *12* (4), 2487−2498.
(27) Xiao, L.; Shan, Y.-L.; Sui, Z.-J.; Chen, D.; Zhou, X.-G.; Yuan, W.-K.; Zhu, Y.-A. Beyond the Reverse Horiuti−Polanyi Mechanism in Propane Dehydrogenation over Pt Catalysts. *ACS Catal.* **2020**, *10* (24), 14887−14902.
(28) van Duin, A. C. T.; Dasgupta, S.; Lorant, F.; Goddard, W. A. ReaxFF: A Reactive Force Field for Hydrocarbons. *J. Phys. Chem. A* **2001**, *105* (41), 9396−9409.
(29) Senftle, T. P.; Hong, S.; Islam, M. M.; Kylasa, S. B.; Zheng, Y.; Shin, Y. K.; Junkermeier, C.; Engel-Herbert, R.; Janik, M. J.; Aktulga, H. M.; et al. The ReaxFF Reactive Force-Field: Development, Applications and Future Directions. *npj Comput. Mater.* **2016**, *2* (1), No. 15011, DOI: 10.1038/npjcompumats.2015.11.
(30) Chenoweth, K.; van Duin, A. C. T.; Goddard, W. A. ReaxFF Reactive Force Field for Molecular Dynamics Simulations of Hydrocarbon Oxidation. *J. Phys. Chem. A* **2008**, *112* (5), 1040−1053.
(31) Leven, I.; Hao, H.; Tan, S.; Guan, X.; Penrod, K. A.; Akbarian, D.; Evangelisti, B.; Hossain, M. J.; Islam, M. M.; Koski, J. P.; et al. Recent Advances for Improving the Accuracy, Transferability, and Efficiency of Reactive Force Fields. *J. Chem. Theory Comput.* **2021**, *17* (6), 3237−3251.
(32) Liang, T.; Shin, Y. K.; Cheng, Y.-T.; Yilmaz, D. E.; Vishnu, K. G.; Verners, O.; Zou, C.; Phillpot, S. R.; Sinnott, S. B.; van Duin, A. C. T. Reactive Potentials for Advanced Atomistic Simulations. *Annu. Rev. Mater. Res.* **2013**, *43* (1), 109−129.
(33) Shin, Y. K.; Shan, T.-R.; Liang, T.; Noordhoek, M. J.; Sinnott, S. B.; van Duin, A. C. T.; Phillpot, S. R. Variable Charge Many-Body Interatomic Potentials. *MRS Bull.* **2012**, *37* (5), 504−512.
(34) Fonseca, A. F.; Lee, G.; Borders, T. L.; Zhang, H.; Kemper, T. W.; Shan, T.-R.; Sinnott, S. B.; Cho, K. Reparameterization of the REBO-CHO Potential for Graphene Oxide Molecular Dynamics Simulations. *Phys. Rev. B* **2011**, *84* (7), 546.
(35) Stuart, S. J.; Tutein, A. B.; Harrison, J. A. A Reactive Potential for Hydrocarbons with Intermolecular Interactions. *J. Chem. Phys.* **2000**, *112* (14), 6472−6486.
(36) Liu, C.; Tao, H.; Lian, C.; Liu, H. Molecular Insights into Guaiacols Hydrodeoxygenation on Nickel Nanoparticle Surfaces. *J. Phys. Chem. C* **2022**, *126* (23), 9724−9735.
(37) Fu, J.; Liu, C.; Li, Y.; Gong, H. ReaxFF Reactive Molecular Dynamics Study on Methanation Reaction from Syngas. *J. Phys. Chem. C* **2023**, *127* (18), 8557−8575.
(38) Van Etten, M. P. C.; De Laat, M. E.; M Hensen, E. J. M.; Ivo, A. W.; Filot, I. A. W. Unraveling the Role of Metal−Support Interactions on the Structure Sensitivity of Fischer−Tropsch Synthesis. *J. Phys. Chem. C* **2023**, *126* (31), 15148−15156, DOI: 10.1021/acs.jpcc.3c02240.
(39) Wang, M.; You, X. Pyrene Adsorption on the Surface of an Iron Oxide Nanoparticle: A ReaxFF Molecular Dynamics Study. *Proc. Combust. Inst.* **2023**, *39* (1), 1157−1164.
(40) Lee, H. W.; Jeong, G.-U.; Kim, M.-C.; Kim, D.; Kim, S.; Han, S. S. Atomistic Origin of Mechanochemical NH_3 Synthesis on Fe Catalysts. *Int. J. Hydrogen Energy* **2023**, *48* (10), 3931−3941.
(41) Monti, S.; Corozzi, A.; Fristrup, P.; Joshi, K. L.; Shin, Y. K.; Oelschlaeger, P.; van Duin, A. C. T.; Barone, V. Exploring the Conformational and Reactive Dynamics of Biomolecules in Solution Using an Extended Version of the Glycine Reactive Force Field. *Phys. Chem. Chem. Phys.* **2013**, *15* (36), 15062.
(42) Deng, L.; Miura, H.; Shishido, T.; Wang, Z.; Hosokawa, S.; Teramura, K.; Tanaka, T. Elucidating Strong Metal-Support Interactions in Pt-Sn/SiO_2 Catalyst and Its Consequences for Dehydrogenation of Lower Alkanes. *J. Catal.* **2018**, *365*, 277−291.
(43) Neyts, E. C.; Ostrikov, K.; Han, Z. J.; Kumar, S.; van Duin, A. C. T.; Bogaerts, A. Defect Healing and Enhanced Nucleation of Carbon Nanotubes by Low-Energy Ion Bombardment. *Phys. Rev. Lett.* **2013**, *110* (6), No. 065501.
(44) Pang, Y.; Zhu, X.; Li, N.; Wang, Z. Investigation on Reaction Mechanism for CO_2 Gasification of Softwood Lignin by ReaxFF MD Method. *Energy* **2023**, *267*, No. 126533.
(45) Kresse, G.; Hafner, J. Ab Initio Molecular Dynamics for Liquid Metals. *Phys. Rev. B* **1993**, *47* (1), 558−561.
(46) Kresse, G.; Furthmuller, J. Efficiency of Ab-Initio Total Energy Calculations for Metals and Semiconductors Using a Plane-Wave Basis Set. *Comput. Mater. Sci.* **1996**, *6* (1), 15−50.
(47) Hohenberg, P.; Kohn, W. Inhomogeneous Electron Gas. *Phys. Rev.* **1964**, *136* (3B), B864−B871.
(48) Kohn, W.; Sham, L. J. Self-Consistent Equations Including Exchange and Correlation Effects. *Phys. Rev.* **1965**, *140* (4A), A1133−A1138.
(49) Hammer, B.; Hansen, L. B.; Norskov, J. K. Improved Adsorption Energetics within Density-Functional Theory Using

Revised Perdew-Burke-Ernzerhof Functionals. *Phys. Rev. B* **1999**, *59* (11), 7413−7421.
(50) Kresse, G.; Joubert, D. From Ultrasoft Pseudopotentials to the Projector Augmented-Wave Method. *Phys. Rev. B* **1999**, *59* (3), 1758−1775.
(51) Monkhorst, H. J.; Pack, J. D. Special Points for Brillouin-Zone Integrations. *Phys. Rev. B* **1976**, *13* (12), 5188−5192.
(52) Methfessel, M.; Paxton, A. T. High-Precision Sampling for Brillouin-Zone Integration in Metals. *Phys. Rev. B* **1989**, *40* (6), 3616−3621.
(53) Álvarez-Moreno, M.; de Graaf, C.; Lopez, N.; Maseras, F.; Poblet, J. M.; Bo, C. Managing the Computational Chemistry Big Data Problem: The ioChem-BD Platform. *J. Chem. Inf. Model.* **2015**, *55*, 95−103, DOI: 10.1021/ci500593j.
(54) Abell, G. C. Empirical Chemical Pseudopotential Theory of Molecular and Metallic Bonding. *Phys. Rev. B* **1985**, *31* (10), 6184−6196.
(55) Tersoff, J. New Empirical Approach for the Structure and Energy of Covalent Systems. *Phys. Rev. B* **1988**, *37* (12), 6991−7000.
(56) Tersoff, J. Empirical Interatomic Potential for Carbon, with Applications to Amorphous Carbon. *Phys. Rev. Lett.* **1988**, *61* (25), 2879−2882.
(57) Brenner, D. W. Empirical Potential for Hydrocarbons for Use in Simulating the Chemical Vapor Deposition of Diamond Films. *Phys. Rev. B* **1990**, *42* (15), 9458−9471.
(58) Mortier, W. J.; van Genechten, K.; Gasteiger, J. Electronegativity Equalization: Application and Parametrization. *J. Am. Chem. Soc.* **1985**, *107* (4), 829−835.
(59) Mortier, W. J.; Ghosh, S. K.; Shankar, S. Electronegativity-Equalization Method for the Calculation of Atomic Charges in Molecules. *J. Am. Chem. Soc.* **1986**, *108* (15), 4315−4320.
(60) Liu, D. C.; Nocedal, J. On the Limited Memory BFGS Method for Large Scale Optimization. *Math. Program.* **1989**, *45* (1−3), 503−528.
(61) Berendsen, H. J. C.; Postma, J. P. M.; van Gunsteren, W. F.; DiNola, A.; Haak, J. R. Molecular Dynamics with Coupling to an External Bath. *J. Chem. Phys.* **1984**, *81* (8), 3684−3690.
(62) Hansen, N.; Ostermeier, A. Completely Derandomized Self-Adaptation in Evolution Strategies. *Evol. Comput.* **2001**, *9* (2), 159−195.
(63) Hansen, N.; Müller, S. D.; Koumoutsakos, P. Reducing the Time Complexity of the Derandomized Evolution Strategy with Covariance Matrix Adaptation (CMA-ES). *Evol. Comput.* **2003**, *11* (1), 1−18.
(64) Hansen, N.; Kern, S. Evaluating the CMA Evolution Strategy on Multimodal Test Functions. In *Lecture Notes in Computer Science*; Springer: Berlin, 2004; pp 282−291.
(65) Igel, C.; Hansen, N.; Roth, S. Covariance Matrix Adaptation for Multi-Objective Optimization. *Evol. Comput.* **2007**, *15* (1), 1−28.
(66) Sanz-Navarro, C. F.; Åstrand, P.-O.; Chen, D.; Rønning, M.; van Duin, A. C. T.; Jacob, T.; Goddard, W. A. Molecular Dynamics Simulations of the Interactions between Platinum Clusters and Carbon Platelets. *J. Phys. Chem. A* **2008**, *112* (7), 1392−1402.
(67) Gai, L.; Shin, Y. K.; Raju, M.; van Duin, A. C. T.; Raman, S. Atomistic Adsorption of Oxygen and Hydrogen on Platinum Catalysts by Hybrid Grand Canonical Monte Carlo/Reactive Molecular Dynamics. *J. Phys. Chem. C* **2016**, *120* (18), 9780−9793.
(68) Shin, Y. K.; Gai, L.; Raman, S.; van Duin, A. C. T. Development of a ReaxFF Reactive Force Field for the Pt−Ni Alloy Catalyst. *J. Phys. Chem. A* **2016**, *120* (41), 8044−8055.
(69) Zhu, W.; Gong, H.; Han, Y.; Zhang, M.; van Duin, A. C. T. Development of a Reactive Force Field for Simulations on the Catalytic Conversion of C/H/O Molecules on Cu-Metal and Cu-Oxide Surfaces and Application to Cu/CuO-Based Chemical Looping. *J. Phys. Chem. C* **2020**, *124* (23), 12512−12520.
(70) Zhao, Z.-J.; Liu, S.; Zha, S.; Cheng, D.; Studt, F.; Henkelman, G.; Gong, J. Theory-Guided Design of Catalytic Materials Using Scaling Relationships and Reactivity Descriptors. *Nat. Rev. Mater.* **2019**, *4* (12), 792−804.
(71) Abild-Pedersen, F.; Greeley, J.; Studt, F.; Rossmeisl, J.; Munter, T. R.; Moses, P. G.; Skúlason, E.; Bligaard, T.; Nørskov, J. K. Scaling Properties of Adsorption Energies for Hydrogen-Containing Molecules on Transition-Metal Surfaces. *Phys. Rev. Lett.* **2007**, *99* (1), No. 016105.
(72) Wang, S.; Petzold, V.; Tripkovic, V.; Kleis, J.; Howalt, J. G.; Skúlason, E.; Fernández, E. M.; Hvolbæk, B.; Jones, G.; Toftelund, A.; Falsig, H.; Björketun, M.; Studt, F.; Abild-Pedersen, F.; Rossmeisl, J.; Nørskov, J. K.; Bligaard, T. Universal Transition State Scaling Relations for (de)Hydrogenation over Transition Metals. *Phys. Chem. Chem. Phys.* **2011**, *13* (46), 20760.
(73) Vandermause, J.; Xie, Y.; Lim, J. S.; Owen, C. J.; Kozinsky, B. Active Learning of Reactive Bayesian Force Fields Applied to Heterogeneous Catalysis Dynamics of H/Pt. *Nat. Commun.* **2022**, *13* (1), No. 5183.
(74) Zhang, W.; Wang, H.; Jiang, J.; Sui, Z.; Zhu, Y.; Chen, D.; Zhou, X. Size Dependence of Pt Catalysts for Propane Dehydrogenation: From Atomically Dispersed to Nanoparticles. *ACS Catal.* **2020**, *10* (21), 12932−12942.
(75) Shan, Y.-L.; Zhu, Y.-A.; Sui, Z.-J.; Chen, D.; Zhou, X.-G. Insights into the Effects of Steam on Propane Dehydrogenation over a Pt/Al_2O_3 Catalyst. *Catal. Sci. Technol.* **2015**, *5* (8), 3991−4000.